

MALDI Imaging on Tissue Microarrays Identifies Molecular Features Associated with Renal Cell Cancer Phenotype

STEFAN STEURER^{1*}, AHMAD SHOAIB SEDDIQI^{1*}, JULIUS MAGNUS SINGER¹, AHMAD SOLIAMAN BAHAR¹, CHRISTIAN EICHELBERG², MICHAEL RINK², ROLAND DAHLEM², HARTWIG HULAND³, GUIDO SAUTER¹, RONALD SIMON¹, SARAH MINNER¹, EIKE BURANDT¹, PHILLIP R. STAHL¹, THORSTEN SCHLOMM³, MARCUS WURLITZER⁴ and HARTMUT SCHLÜTER⁴

¹Institute of Pathology, ²Department of Urology, ³Martini Clinic, and

⁴Institute of Clinical Chemistry at the University Medical Center Hamburg-Eppendorf, Hamburg, Germany

Abstract. *Aim: To identify molecular features associated with clinico-pathological parameters in renal cell cancer. Materials and Methods: Matrix-assisted laser desorption/ionization (MALDI) mass spectrometry imaging was employed for a kidney cancer tissue microarray containing tissue samples from 789 patients for which clinical follow-up data were available. Results: A comparison of mass spectrometric signals with clinico-pathological features revealed significant differences between papillary and clear cell renal cell cancer. Within the subgroup of clear cell RCC, statistical associations with tumor stage (seven signals, $p < 0.01$ each), Fuhrman grade (seven signals, $p < 0.0001$ each), and presence of lymph node metastases (10 signals, $p < 0.01$ each) were found. In addition, the presence of one signal was significantly linked to shortened patient survival ($p = 0.0198$). Conclusion: Our data pinpoint towards various molecules with potential relevance in renal cell cancer. They also demonstrate that the combination of the MALDI mass spectrometry imaging and large-scale tissue microarray platforms represents a powerful approach to identify clinically-relevant molecular cancer features.*

Renal cell carcinoma (RCC) accounts for more than 80% of renal tumors. Its incidence is rising steadily by 2-4% per year, making it now the seventh most common cancer type (1). In the US, more than 60,000 new cases have been

diagnosed in 2010 and about 15,000 patients have died from their cancers (1). The molecular mechanisms underlying disease progression are still largely unknown. Accordingly, molecular markers allowing for a prediction of the clinical course of this disease are missing.

Molecular prognostic markers can only be identified if large and clinically well-defined patient cohorts are available for molecular analyses. The tissue microarray (TMA) technology has become a standard tool for large-scale tissue analysis allowing for parallel analysis of hundreds of tissue samples in one experiment (2). However, 'classical' TMA analysis using for example immunohistochemistry to identify protein expression is limited by the fact that usually only one protein can be analyzed on one slide and at the same time. Matrix-assisted laser desorption/ionization (MALDI) mass spectrometry imaging (MSI) is a promising tool for the high-throughput analysis of molecular features, including multiple different peptides and proteins, in one experiment (3). A combination of both approaches, *i.e.* the TMA and MALDI-MSI technology, thus enables for both, large-scale and highly paralleled screening of patient tissues.

In the present study, we have employed MALDI-MSI to search for tumor-associated masses in a set of TMAs including 789 kidney carcinomas. We found a multitude of m/z signals associated with different features of renal cell cancer, including stage, grade, histological subtype, as well as patient prognosis, some of which may have potential for clinical relevance.

Materials and Methods

Tissues. Two TMA sections containing one formalin-fixed and paraffin-embedded tissue punch (diameter 0.6 mm) each from 978 patients with kidney cancer undergoing surgery between 1970 and 2005 at the Departments of Urology in Hamburg (Germany) and Basel (Switzerland) were included in this study. Presence of tumor cells in the tissue spots was confirmed by visual inspection of the hematoxylin and eosin-stained slides after MALDI-MSI analysis. A total of 189 tissue spots were excluded from analysis

*These Authors contributed equally to this work.

Correspondence to: Professor Dr. Hartmut Schlüter, Institute of Clinical Chemistry, University Medical Center Hamburg-Eppendorf, Bldg. N27, Room 00.008, Martinistr. 52, 20246 Hamburg, Germany. Tel: +49 40741058795, Fax: +49 4041040097, e-mail: hschluet@uke.de

Key Words: MALDI mass spectrometry imaging, MALDI-MSI, tissue microarray, renal cell cancer, biomarker.

because they were either lacking cancer cells or completely absent in the TMA sections. The pathological and clinical parameters of the remaining 789 tumors included in this study are described in Table I.

Sample preparation, matrix deposition, and MALDI-MSI analysis. The MALDI procedure used in this study had been previously described in detail (4). In brief, 6 µm TMA sections were mounted onto indium-tin-oxide (ITO)-coated conductive glass slides (Bruker Daltonics, Bremen, Germany) and air-dried. After deparaffinization and antigen retrieval in pH 2 buffer (Retrieval TM2, Target Retrieval Solution 10X; Biogenex, Fremont, CA, USA), slides were covered with trypsin solution (20 µg porcine Trypsin in 200 µl of 40 mM ammonium bicarbonate) using an ImagePrep device (Bruker Daltonics). Digital images of the slides and the tissues were obtained using a flatbed scanner before the matrix was deposited. The matrix solution [400 mg 2,5-dihydroxybenzoic acid (DHB; Bruker Daltonics) in 13,3 ml 50% methanol/water and 1% trifluoroacetic acid] was sprayed onto the sample using an ImagePrep device (Bruker Daltonics). Mass spectra were acquired using an autoflex speed MALDI time of flight mass spectrometer (Bruker Daltonics) equipped with a smartbeam II laser and controlled by the flexControl 3.3 software package. Spectra were acquired in positive reflectron mode in an m/z range of 500-3680 at a sampling rate of 1.0 GS/s. A total of 500 single spectra per pixel at a laser shot frequency of 1000 Hz at constant laser power were accumulated. Each spot position was systematically analyzed row by row to sample the entire spot area with a lateral resolution of 80 µm. Data analysis and image generation was carried out with flexImaging 3.0 (Bruker Daltonics). The total ion current of each spectrum was used for signal intensity normalization. Following MSI analysis, the matrix was removed, and the hematoxylin and eosin-stained slides were scanned in order to spatially relate the signal intensities to histological structures in the individual tissue spots. Only signals that typically co-localized with cancer cells were classified.

Data analysis. Selection of peaks was performed with flexAnalysis on every single spectrum. The signal list for each spectrum was exported and loaded into in-house software to be prepared for statistical analysis. For each signal, the average intensity was calculated for each TMA spot, and TMA spots were classified as negative or positive by unsupervised clustering. The clustering algorithm automatically determined the optimal thresholds between negative and positive for each signal using the local optimization method. The clustering results were correlated to clinical data using the JMP software package (SAS Institute Inc., Cary, NC, USA).

Statistics. For statistical analysis we used the JMP 9.0.2 software. Contingency tables were calculated to study the association between the presence or absence of selected signals and tumor stage and grade, as well as other clinico-pathological variables, and the Chi-square (likelihood) test was used to find significant relationships. Kaplan–Meier curves were generated for overall survival. The log-rank test was applied to test the significance of differences between stratified survival functions. Cox proportional hazards regression analysis was performed to test the statistical independence and significance between pathological, molecular, and clinical variables.

Table I. Pathological and clinical data of the arrayed kidney carcinomas.

	No. of patients Study cohort on TMA (n=789)
Mean follow up (months)	59.5
Age (years)	
<50	106
50-60	220
61-70	266
>70	193
Gender	
Male	482
Female	303
Histology	
Clear Cell	528
Chromophobic	41
Papillary	112
Other types*	42
pT category	
pT1	298
pT2	120
pT3-4	299
Grade category	
1	95
2	279
≥3	244
pN category	
pN0	344
pN1	56

Numbers do not always add up to 789 in the different categories because of cases with missing data. *Including sarcomatoid cancers and unknown histologies.

Results

Technical issues. A total of 25 distinct MALDI-MSI signals corresponding to cancer cells were identified in the current study. The signals were found in 4.4-76.3% of the 789 arrayed carcinomas, ranging from m/z 603.7 to m/z 3315.5, including m/z 603.7, 604.2, 614.9, 616.4, 619.4, 631.5, 644.8, 649.6, 675.7, 803.9, 805.8, 945.1, 1032.3, 1047.0, 1105.4, 1179.0, 1198.8, 1274.6, 1459.9, 1477.7, 1529.6, 2056.2, 2728.7, 2960.3, and 3315.5. Representative images of MALDI analysis are shown in Figure 1.

Signals associated with RCC histology, tumor stage, Fuhrman grade, and presence of nodal metastasis. A comparison of detectable MALDI-MSI signals among the different histological tumor types showed only moderate differences, including two signals that were found more frequently in papillary (40%/35%) and chromophobe cancer (41%/34%) as compared to clear cell carcinoma (30%/25%), namely m/z 1529.6 and 2056.2, but the difference was statistically significant only between papillary and clear cell cancer ($p=0.0371$ for m/z 1529.6 and $p=0.0297$

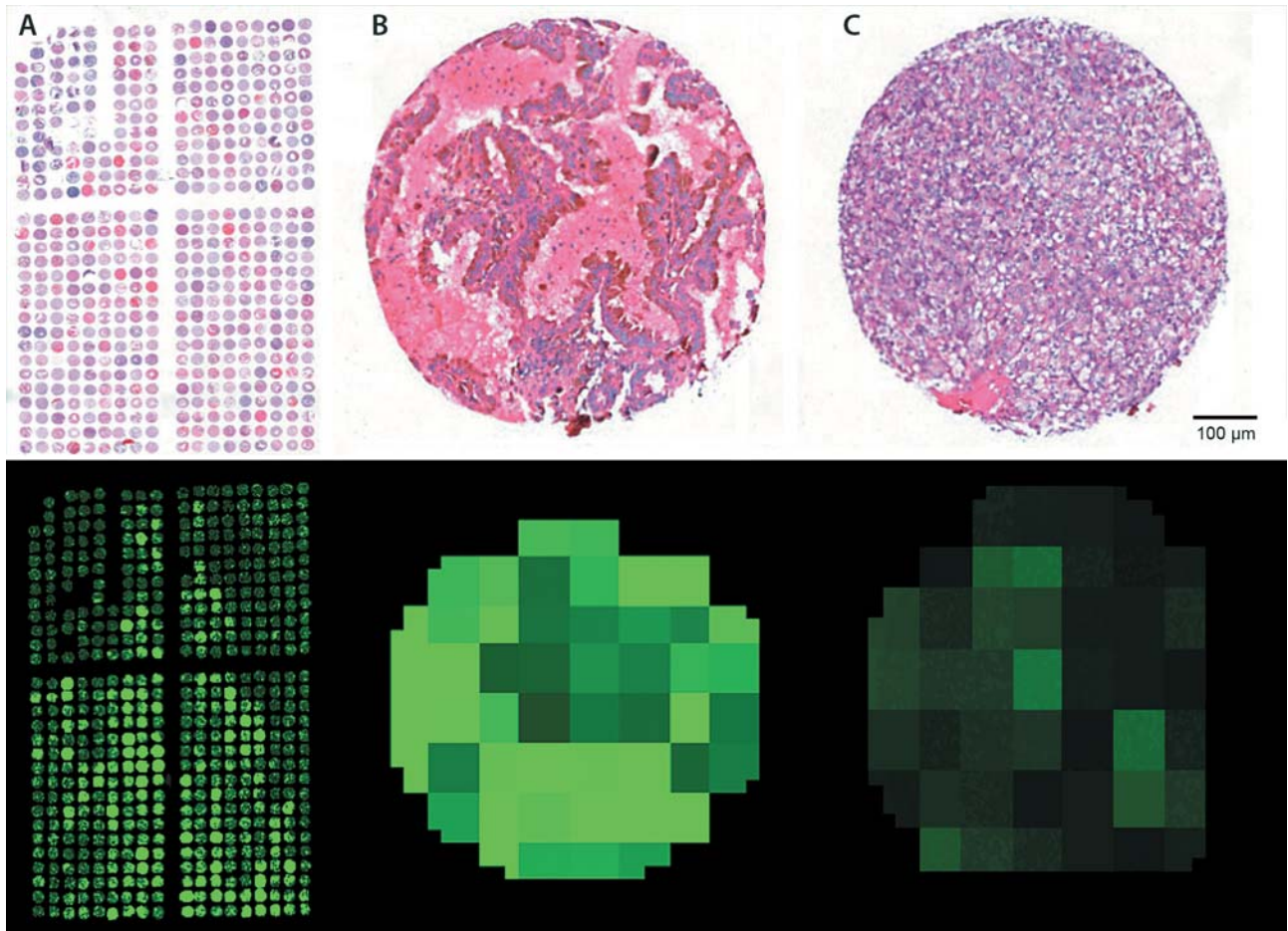


Figure 1. Representative images from matrix-assisted laser desorption/ionization mass spectrometric imaging (MALDI-MSI) analysis. Upper panel: Hematoxylin-eosin staining; lower panel: MALDI-MSI. A: Overview of one tissue microarray slide. B: Magnified image of a papillary kidney cancer tissue spot (diameter 0.6 mm) showing signals with an intensity ranging from dark (negative) to bright (highest) for m/z 631.5. C: Tissue spot of a clear cell renal cell carcinoma virtually lacking signals for m/z 631.5.

for m/z 2056.2, Table II). One additional signal, m/z 1274.6, was substantially less frequently observed in chromophobe (2.4%), compared to papillary (11%, $p=0.0697$) and clear cell cancer (10%, $p=0.0784$), but the difference did not reach statistical significance. Comparisons with tumor stage, Fuhrman grade, and presence of nodal metastasis were limited to clear cell RCC, the only tumor type with sufficient numbers for statistical analyses on our TMA ($n=528$). In clear cell RCC, we found a total of 15 m/z signals that were linked to one or more phenotypic features of RCC. Strongest associations were seen between m/z 603.7, 614.9, 616.4, 1198.8, 1529.6, 2056.2, and 2728.7 and tumor stage ($p<0.01$ each), between m/z 603.7, 614.9, 616.4, 1105.4, 1477.7, 1529.6, and 2728.7 and Fuhrman grade ($p<0.0001$ each), as well as m/z 603.7, 614.9, 616.4, 644.8, 1105.4, 1459.9, 1477.7, 1529.6, 2728.7 and 2960.3 and the presence of lymph node metastases ($p<0.01$ each). All associations are shown in Table III.

Associations with clinical outcome. In order to investigate the prognostic impact of individual m/z signals, we analyzed the associations between presence of individual m/z signals and overall survival in the subset of $n=528$ clear cell RCC. The presence of one signal, m/z 1105.4, was significantly linked to shortened overall patient survival in univariate analysis ($p=0.0198$, Figure 2), but not in a multivariate analysis including the established prognosticators pT stage, Fuhrman grade, and nodal stage ($p=0.0879$, Table IV).

Discussion

In our study, we applied MALDI-MSI to a tissue microarray including 789 kidney carcinomas. The results of this analysis identified distinct signals linked to RCC histology, tumor progression, and patient prognosis.

Table II. Associations between m/z signals and histological kidney cancer subtype.

m/z	Clear cell (n=528)	Papillary (n=112)	Chromophobe (n=41)	p-Value		
				Clear cell vs. papillary	Clear cell vs. chromophobe	Papillary vs. chromophobe
603.7	44.3	45.5	39.0	0.8139	0.5087	0.4707
604.2	28.4	29.5	31.7	0.8228	0.6557	0.7894
614.9	37.3	37.5	36.6	0.9700	0.9262	0.9174
616.4	46.4	50.0	36.6	0.4886	0.2207	0.1384
619.2	53.2	46.4	46.3	0.1915	0.3959	0.9924
631.5	55.3	58.9	65.9	0.4817	0.1850	0.4345
644.8	54.7	55.4	51.2	0.9043	0.6637	0.6494
649.6	28.8	37.5	39.0	0.0727	0.1766	0.8635
675.7	65.0	67.0	73.2	0.6851	0.2775	0.4595
803.9	60.0	56.3	63.4	0.4598	0.6690	0.4241
805.8	55.3	58.0	63.4	0.5963	0.3100	0.5468
945.1	75.4	77.7	73.2	0.6032	0.7544	0.5641
1032.3	45.8	44.6	46.3	0.8182	0.9499	0.8517
1047.0	15.9	15.2	22.0	0.8466	0.3316	0.3334
1105.4	65.2	68.8	56.1	0.4633	0.2496	0.1493
1179.0	18.6	21.4	24.4	0.4879	0.3735	0.6983
1198.8	56.1	63.4	53.7	0.1517	0.7657	0.2773
1274.6	9.5	10.7	2.4	0.6894	0.0784	0.0697
1459.9	48.1	46.4	58.5	0.7468	0.1974	0.1838
1477.7	34.9	34.8	36.6	0.9956	0.8228	0.8400
1529.6	29.9	40.2	41.5	0.0371	0.1323	0.8861
2056.2	24.6	34.8	34.2	0.0297	0.1898	0.9380
2728.7	32.2	30.4	24.4	0.7033	0.2899	0.4654
2960.3	19.3	14.3	22.0	0.2006	0.6861	0.2677
3315.5	4.9	4.5	4.9	0.8352	0.9895	0.9142

Significant p-values are indicated by bold face type.

Differences between histological tumor types included two signals, m/z 1529.6 and 2056.2, that occurred significantly less frequently in clear cell cancer compared to papillary RCC, the two histological subtypes that were the majority (89%) of the analyzed samples. No significant differences were found between clear cell or papillary cancer and chromophobe carcinoma. This was surprising given that these tumors originate from different cell types including the epithelium of the proximal tubules (clear cell RCC and papillary RCC) and the distal tubules (chromophobe RCC). The lack of detectable differences in the m/z patterns between these histological types may first of all be related to the comparatively small number of chromophobe RCC (n=41) included in this study. However, m/z 1264.6 was substantially less frequent in chromophobic (2%) compared to clear cell (10%) or papillary (11%) cancer. It is, therefore, possible that this signal is related to molecular features that are characteristic for cells of the proximal tubules.

We detected three signals, presence (m/z 644.8 and 2728.7) or absence (m/z 1179.0) which were linked to locally advanced (pT3-4) and high grade (G3-4) cancer in our study. Since these types of cancer have a poor prognosis, it was not

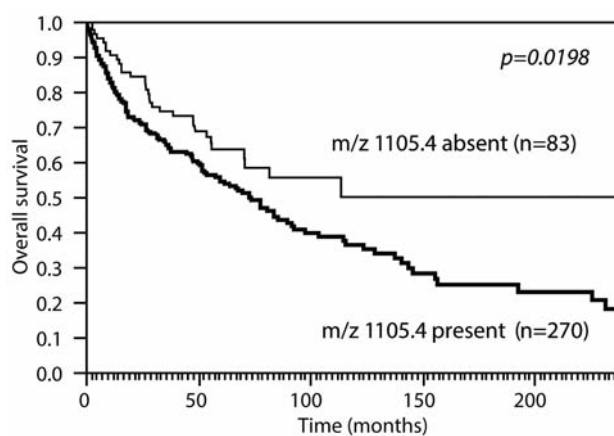


Figure 2. Kaplan–Meier plot showing a significant association between the presence of m/z 1105.4 and poor overall survival.

surprising that two of those signals, m/z 644.8 and 2728.7, were also linked to the presence of lymph node metastases. These markers might serve to identify patients at risk for tumor recurrence and progression after surgery for organ-

Table III. Associations between m/z signals and kidney cancer phenotype in 528 cases of clear cell kidney cancer.

m/z	Stage				Fuhrman Grade				Nodal stage		
	1 n=212	2 n=74	3-4 n=234	p-Value	1 n=72	2 n=206	3-4 n=199	p-Value	N0 n=210	N+ n=32	p-Value
603.7	36.32%	50.00%	50.85%	0.0052	19.44%	42.23%	60.30%	<0.0001	30.48%	59.38%	0.0018
604.2	28.77%	28.38%	29.06%	0.9932	20.83%	29.61%	31.16%	0.2267	21.90%	21.88%	0.997
614.9	45.75%	39.19%	27.78%	0.0004	63.89%	40.78%	15.58%	<0.0001	60.95%	15.63%	<0.0001
616.4	55.19%	40.54%	39.32%	0.0021	66.67%	51.94%	25.63%	<0.0001	64.29%	25.00%	<0.0001
619.2	52.83%	52.70%	52.99%	0.9988	45.83%	53.40%	53.77%	0.4783	55.24%	53.13%	0.8231
631.5	52.36%	58.11%	57.26%	0.5113	51.39%	55.34%	58.79%	0.527	51.90%	50.00%	0.8408
644.8	48.58%	51.35%	62.39%	0.0104	47.22%	52.91%	63.32%	0.0249	39.52%	68.75%	0.0019
649.6	30.66%	32.43%	24.79%	0.2670	25.00%	30.58%	27.64%	0.622	30.95%	21.88%	0.2832
675.7	63.68%	59.46%	69.23%	0.2298	62.50%	65.53%	66.33%	0.8426	57.62%	71.88%	0.1186
803.9	60.85%	59.46%	59.83%	0.9667	63.89%	56.80%	61.81%	0.4481	60.95%	56.25%	0.6141
805.8	58.96%	51.35%	53.42%	0.3763	70.83%	51.94%	51.76%	0.0101	60.95%	53.13%	0.403
945.1	75.47%	70.27%	77.78%	0.4279	73.61%	78.16%	74.87%	0.6406	69.52%	81.25%	0.1575
1032.3	43.40%	37.84%	51.28%	0.0741	34.72%	44.66%	54.77%	0.0079	42.38%	50.00%	0.4196
1047.0	18.87%	13.51%	14.10%	0.3257	11.11%	15.53%	18.09%	0.3562	10.00%	18.75%	0.1707
1105.4	65.57%	55.41%	69.23%	0.0970	48.61%	62.14%	80.40%	<0.0001	43.81%	81.25%	<0.0001
1179.0	19.81%	28.38%	14.53%	0.0287	19.44%	23.30%	13.07%	0.0266	18.57%	28.13%	0.224
1198.8	62.26%	40.54%	56.41%	0.0053	52.78%	57.77%	58.79%	0.6724	43.33%	56.25%	0.1724
1274.6	11.79%	9.46%	7.26%	0.2622	12.50%	9.71%	8.54%	0.6344	7.62%	6.25%	0.7786
1459.9	49.53%	45.95%	48.29%	0.8663	43.06%	43.69%	57.79%	0.0087	36.19%	68.75%	0.0005
1477.7	35.85%	29.73%	36.32%	0.5585	25.00%	27.67%	50.25%	<0.0001	20.48%	56.25%	<0.0001
1529.6	37.26%	27.03%	23.93%	0.0078	61.11%	33.50%	9.55%	<0.0001	50.48%	15.63%	0.0001
2056.2	31.60%	14.86%	21.37%	0.0043	27.78%	27.67%	19.10%	0.0918	29.05%	43.75%	0.1023
2728.7	26.42%	25.68%	40.17%	0.0033	19.44%	26.21%	48.24%	<0.0001	19.52%	53.13%	0.0001
2960.3	17.92%	16.22%	21.37%	0.5070	8.33%	21.36%	22.61%	0.0141	15.71%	46.88%	0.0002
3315.5	6.13%	2.70%	4.70%	0.4584	4.17%	7.28%	3.52%	0.2157	4.29%	3.13%	0.7499

Significant p-values are indicated by bold face type. Data on stage, grade and nodal stage were not available for all tumors.

confined tumors, and potentially also guide therapy towards extensive adjuvant treatment. In addition, we found one signal, m/z 1105.4, which was linked to adverse prognosis in univariate analysis. This finding may be of clinical importance given the disparate clinical characteristics of kidney cancer which make it difficult to predict the clinical course solely based on the established prognostic markers pT stage, Fuhrmann grade, and nodal stage. Little is known on the genetic alterations associated with kidney cancer progression. A multitude of putative prognostic markers has been suggested [reviewed in (5)]. For example, loss of the cell-cycle regulator p21 has been linked to the development of metastatic disease (6), inactivation of p53 had been associated with tumor recurrence and worse prognosis (7, 8), and low expression of carbonic anhydrase IX (CA-IX) (9) and hypoxia-inducible factor 1-alpha (10), as well as overexpression of extracellular signal-regulated kinase (11) and caveolin-1 (12, 13) have been linked to shortened patient survival. However, none of these was proven to be sufficiently reliable to justify the development of a diagnostic routine test. Our findings further support the concept that clinically-

Table IV. Multivariate analysis including the established risk factors pT stage, Fuhrman grade and nodal stage, in addition to m/z 1105.4.

Parameter		RR	95% CI	p-Value
pT	pT2 vs. pT1	1.5	0.6-4.2	0.1692
	pT3-4 vs. pT2	1.7	0.8-3.9	
Grade	G2 vs. G1	1.5	0.6-4.2	0.6308
	G3-4 vs. G2	1.0	0.6-1.8	
pN	pN+ vs. pN0	3.3	1.7-6.2	0.0009
m/z 1105.4 Signal	Positive vs. negative.	1.7	0.9-3.3	0.0879

RR: Risk ratio, CI: confidence interval.

suitable markers may exist, and it will be interesting to identify the molecules underlying the m/z signals.

Several previous studies have analyzed kidney cancer cases using MALDI. Junker *et al.* analyzed stage-related protein alterations in kidney cancer using MALDI-TOF-MS/MS for protein identification in a study on 27 patients with cancer (14). Oppenheimer *et al.* (15) used MALDI/MS

of snap-frozen tissue from 75 patients with clear cell RCC to show the characteristics of tumor margins and the tumor microenvironment (15). Chinello *et al.* identified a cluster of three peptides that were able to discriminate 33 patients with clear cell RCC from 29 healthy controls using the ClinProt/MALDI-TOF technique (16). Yang *et al.* identified cyclophilin A as a potential prognostic factor for ccRCC using MALDI-TOF/MS in a study with 81 patients primary clear cell RCC (17).

In a recent study, we identified m/z 1502 as a marker for early recurrence in prostate cancer. This finding was also reproduced when a subsequent section of the tissue microarray block was re-analyzed (4). As MALDI imaging is a relatively simple tool that can easily be applied in routine settings, our findings raise the hope that this approach may be better suited for routine application than DNA or RNA analysis, or even immunohistochemistry, which is notorious for reproducibility issues between laboratories (18).

The data of this study again demonstrate the strong potential of combining the MALDI-MSI and TMA techniques. MALDI-MSI is optimally suited to screen a given tissue sample for a large number of molecular features within one experiment, including for example peptides, lipids, or metabolites. TMA technology allows for analysis of hundreds of tissue samples on the same slide. Whereas typical *in situ* techniques applied to TMAs, including immunohistochemistry or fluorescence *in situ* analysis, allow for the analysis of only one parameter at a time, MALDI-MSI multiplies the number of parameters that can be measured. Since the relevant areas of the tissues to be analyzed are selected by a pathologist during TMA construction, MALDI-MSI analysis can be limited to a small area of individual tissues, *i.e.* a single 0.6 mm TMA spot, so that the total time required for analysis of a typical TMA section is not significantly different from that required for analysis of a single large section.

Whereas a multitude of studies analyzed frozen normal and diseased tissues from human and animals [for example (19-23)], only comparatively few studies have employed MALDI-MSI on TMAs, or large sections from formalin-fixed tissues in order to search for associations between molecular features and tumor phenotype. For example, Casadonte *et al.* (24) and Groseclose *et al.* (25) reported MALDI imaging signal patterns that were suitable to separate squamous cell cancers from adenocarcinomas of the lung. Lazova *et al.* described distinct signatures for Spitz naevi and Spitzoid skin cancer (24). Others identified specific proteins, including actin and collagen in ovarian cancer (25), or a 78-kDa glucose-regulated protein in pancreatic cancer (26). The results obtained from these studies further support the concept of MALDI-MSI for high-throughput analysis of formalin-fixed tissues.

The results of our study demonstrate the power of MALDI-MSI in combination with the TMA technology and clinical databases for simultaneously screening for molecular alterations and assessing their clinical value. Given that the TMA technology has developed into the standard tool for *in situ* tissue analysis, and that TMAs including virtually all different types of healthy and diseased formalin-fixed tissues are now broadly available, it can be expected that the number of studies applying MALDI-MSI to such TMAs will steadily increase in the future. Importantly, large TMAs with their associated clinical data will – at the same time – provide validation of the clinical impact of the identified markers.

References

- Jemal A, Siegel R, Xu J and Ward E: Cancer statistics, 2010. *CA Cancer J Clin* 60: 277-300, 2010.
- Kononen J, Bubendorf L, Kallioniemi A, Barlund M, Schraml P, Leighton S, Torhorst J, Mihatsch MJ, Sauter G and Kallioniemi OP: Tissue microarrays for high-throughput molecular profiling of tumor specimens. 4: 844-847, 1998.
- Cornett DS, Reyzer ML, Chaurand P and Caprioli RM: MALDI imaging mass spectrometry: molecular snapshots of biochemical systems. 4: 828-833, 2007.
- Steurer S, Borkowski C, Odinga S, Buchholz M, Koop C, Huland H, Becker M, Witt M, Trede D, Omidi M, Kraus O, Bahar AS, Seddiqi AS, Singer JM, Kwiatkowski M, Trusch M, Simon R, Wurlitzer M, Minner S, Schlomm T, Sauter G and Schluter H: MALDI mass spectrometric imaging based identification of clinically relevant signals in prostate cancer using large-scale tissue microarrays. *Int J Cancer* 133: 920-928, 2013.
- Lam JS, Klatte T, Kim HL, Patard JJ, Breda A, Zisman A, Pantuck AJ and Figlin RA: Prognostic factors and selection for clinical studies of patients with kidney cancer. *Crit Rev Oncol Hematol* 65: 235-262, 2008.
- Weiss RH, Borowsky AD, Seligson D, Lin PY, Dillard-Telm L, Belldegrin AS, Figlin RA and Pantuck AD: p21 is a prognostic marker for renal cell carcinoma: implications for novel therapeutic approaches. *J Urol* 177: 63-68; discussion 68-69, 2007.
- Shvarts O, Seligson D, Lam J, Shi T, Horvath S, Figlin R, Belldegrin A and Pantuck AJ: p53 is an independent predictor of tumor recurrence and progression after nephrectomy in patients with localized renal cell carcinoma. *J Urol* 173: 725-728, 2005.
- Kim HL, Seligson D, Liu X, Janzen N, Bui MH, Yu H, Shi T, Figlin RA, Horvath S and Belldegrin AS: Using protein expressions to predict survival in clear cell renal carcinoma. *Clin Cancer Res* 10: 5464-5471, 2004.
- Sandlund J, Oosterwijk E, Grankvist K, Oosterwijk-Wakka J, Ljungberg B and Rasmuson T: Prognostic impact of carbonic anhydrase IX expression in human renal cell carcinoma. *BJU Int* 100: 556-560, 2007.
- Lidgren A, Hedberg Y, Grankvist K, Rasmuson T, Vasko J and Ljungberg B: The expression of hypoxia-inducible factor 1alpha is a favorable independent prognostic factor in renal cell carcinoma. *Clin Cancer Res* 11: 1129-1135, 2005.
- Campbell L, Nuttall R, Griffiths D and Gumbleton M: Activated extracellular signal-regulated kinase is an independent prognostic factor in clinically confined renal cell carcinoma. *Cancer* 115: 3457-3467, 2009.

- 12 Campbell L, Gumbleton M and Griffiths DF: Caveolin-1 overexpression predicts poor disease-free survival of patients with clinically confined renal cell carcinoma. *Br J Cancer* **89**: 1909-1913, 2003.
- 13 Campbell L, Jasani B, Edwards K, Gumbleton M and Griffiths DF: Combined expression of caveolin-1 and an activated AKT/mTOR pathway predicts reduced disease-free survival in clinically confined renal cell carcinoma. *Br J Cancer* **98**: 931-940, 2008.
- 14 Junker H, Venz S, Zimmermann U, Thiele A, Scharf C and Walther R: Stage-related alterations in renal cell carcinoma – comprehensive quantitative analysis by 2D-DIGE and protein network analysis. *PLoS One* **6**: e21867, 2011.
- 15 Oppenheimer SR, Mi D, Sanders ME and Caprioli RM: Molecular analysis of tumor margins by MALDI mass spectrometry in renal carcinoma. *J Proteome Res* **9**: 2182-2190, 2010.
- 16 Chinello C, Gianazza E, Zoppis I, Mainini V, Galbusera C, Picozzi S, Rocco F, Galasso G, Bosari S, Ferrero S, Perego R, Raimondo F, Bianchi C, Pitto M, Signorini S, Brambilla P, Mocarelli P, Galli Kienle M and Magni F: Serum biomarkers of renal cell carcinoma assessed using a protein profiling approach based on ClinProt technique. *Urology* **75**: 842-847, 2010.
- 17 Yang J, Li A, Yang Y and Li X: Identification of cyclophilin A as a potential prognostic factor for clear-cell renal cell carcinoma by comparative proteomic analysis. *Cancer Biol Ther* **11**: 535-546, 2011.
- 18 Gancberg D, Jarvinen T, di Leo A, Rouas G, Cardoso F, Paesmans M, Verhest A, Piccart MJ, Isola J and Larsimont D: Evaluation of HER-2/NEU protein expression in breast cancer by immunohistochemistry: an interlaboratory study assessing the reproducibility of HER-2/NEU testing *74*: 113-120, 2002.
- 19 Le Faouder J, Laouirem S, Chapelle M, Albuquerque M, Belghiti J, Degos F, Paradis V, Camadro JM and Bedossa P: Imaging mass spectrometry provides fingerprints for distinguishing hepatocellular carcinoma from cirrhosis. *J Proteome Res* **10**: 3755-3765, 2011.
- 20 Kriegsmann M, Seeley EH, Schwarting A, Kriegsmann J, Otto M, Thabe H, Dierkes B, Biehl C, Sack U, Wellmann A, Kahaly GJ, Schwamborn K and Caprioli RM: MALDI MS imaging as a powerful tool for investigating synovial tissue. *Scand J Rheumatol* **41**: 305-309, 2012.
- 21 Mark L, Maasz G and Pirger Z: High resolution spatial distribution of neuropeptides by MALDI imaging mass spectrometry in the terrestrial snail, *Helix pomatia*. *Acta Biol Hung* **63(Suppl 2)**: 113-122, 2012.
- 22 Acquadro E, Cabella C, Ghiani S, Miragoli L, Bucci EM and Corpillo D: Matrix-assisted laser desorption ionization imaging mass spectrometry detection of a magnetic resonance imaging contrast agent in mouse liver. *Anal Chem* **81**: 2779-2784, 2009.
- 23 Shanta SR, Choi CS, Lee JH, Shin CY, Kim YJ, Kim KH and Kim KP: Global changes in phospholipids identified by MALDI MS in rats with focal cerebral ischemia. *J Lipid Res* **53**: 1823-1831, 2012.
- 24 Lazova R, Seeley EH, Keenan M, Gueorguieva R and Caprioli RM: Imaging mass spectrometry – a new and promising method to differentiate Spitz nevi from Spitzoid malignant melanomas. *Am J Dermatopathol* **34**: 82-90, 2012.
- 25 Gustafsson JO, Oehler MK, McColl SR and Hoffmann P: Citric acid antigen retrieval (CAAR) for tryptic peptide imaging directly on archived formalin-fixed paraffin-embedded tissue. *J Proteome Res* **9**: 4315-4328, 2010.
- 26 Djidja MC, Claude E, Snel MF, Scriven P, Francese S, Carolan V and Clench MR: MALDI-ion mobility separation-mass spectrometry imaging of glucose-regulated protein 78 kDa (Grp78) in human formalin-fixed, paraffin-embedded pancreatic adenocarcinoma tissue sections. *J Proteome Res* **8**: 4876-4884, 2009.

Received January 13, 2014

Revised March 3, 2014

Accepted March 4, 2014